

# Pole analysis on unitarized $SU(3) \times SU(3)$ one loop $\chi$ PT amplitudes

LING-YUN DAI<sup>1</sup>, X. G. WANG <sup>2</sup>AND H. Q. ZHENG<sup>3</sup>

*Department of Physics and State Key Laboratory of Nuclear Physics and Technology, Peking University, Beijing 100871, P. R. China*

August 9, 2011

## Abstract

We analyze  $\pi\pi - K\bar{K}$  and  $\pi\eta - K\bar{K}$  couple channel [1,1] matrix Padé amplitudes of  $SU(3) \times SU(3)$  chiral perturbation theory. By fitting phase shift and inelasticity data, we determine pole positions in different channels ( $f_0(980)$ ,  $a_0(980)$ ,  $f_0(600)$ ,  $K_0^*(800)$ ,  $K^*(892)$ ,  $\rho(770)$ ) and trace their  $N_c$  trajectories. We stress that a couple channel Breit–Wigner resonance should exhibit two poles on different Riemann sheets that reach the same position on the real axis when  $N_c = \infty$ . Poles are hence classified using this criteria and we conclude that  $K^*(892)$  and  $\rho(770)$  are unambiguous Breit–Wigner resonances. For scalars the situation is much less clear. We find that  $f_0(980)$  is a molecular state rather than a Breit–Wigner resonance, while  $a_0(980)$ , though behaves oddly when varying  $N_c$ , does maintain a twin pole structure.

Key words: Meson – Meson scattering, Unitarity, Hadron resonance

PACS number: 14.40.Be, 11.55.Bq, 11.30.Rd

## 1 Introduction

Chiral perturbation theory [1, 2, 3] has been proven very successful in studying low energy hadron physics. Nevertheless, when the energy goes higher, up to roughly 500MeV, chiral expansion breaks down since it's an expansion in terms of pseudo-goldstone boson mass and external momentum. Much efforts have also been made in exploring physics beyond the validity domain of chiral expansions. However, due to the non-perturbative nature it is very difficult to study the problem in a model independent way.

---

<sup>1</sup>e-mail: daily03@pku.edu.cn

<sup>2</sup>e-mail: wangxuanguang@pku.edu.cn. Address after September 1,2011, Institute of High Energy Physics, Chinese Academy of Science, Beijing 100049

<sup>3</sup>e-mail: zhenghq@pku.edu.cn

When studying physics at higher energies, one of the central question was whether there exists (the lightest) scalar mesons such as  $f_0(600)$  (also called as  $\sigma$ ) and  $K_0^*(800)$  (also called as  $\kappa$ ). Dispersion technique played a crucial role in firmly establishing the very existence of these resonances and in determining their precise pole locations. [4]-[9] However, the property of these scalar resonances, including that of  $f_0(980)$  and  $a_0(980)$ , remains mysterious, e.g., whether they are  $q\bar{q}$  states, or  $qq\bar{q}\bar{q}$  states or molecular states? and what is the role they play in spontaneous chiral symmetry breaking, and even in confinement? When studying the substructure of these scalar mesons, some authors try to investigate the two photon decay width of the resonant states [10]-[14]. One may also get helpful information from the large  $N_c$  behavior of the resonance poles [15]-[20]. The latter depends on the use of the unitarized chiral perturbative amplitudes. It is however known that Padé approximants encounter severe difficulties, e.g., it violates crossing symmetry; it introduces spurious poles on the physical sheet (and on un-physical sheets as well) and hence violates analyticity. Besides these deficiencies, unitarization approaches make correct predictions in some aspects, including the existence of  $f_0(600)$  and  $K_0^*(800)$  resonances.

This paper also devotes to the study of light hadron physics using unitarization approach of  $SU(3) \times SU(3)$   $\chi$ PT. Classification of resonance poles is an important topic in hadron physics. For this reason we point out that a couple channel Breit–Wigner resonance should exhibit two poles on different Riemann sheets and reach the same position on the real axis when  $N_c = \infty$ . This simple criteria is used to classify poles that emerge in the unitarized amplitudes. It is clearly seen that  $K^*(892)$  and  $\rho(770)$  are unambiguous Breit–Wigner resonances, which, in our understanding, is what Padé approximants can predict reliably. This observation encourages us to use this criteria to analyze scalar resonances and we conclude that  $f_0(980)$  is **not** a Breit–Wigner resonance, it is most likely a  $K\bar{K}$  (virtual) bound state when  $N_c$  is large. On the other side,  $a_0(980)$  though behaves oddly when varying  $N_c$ , does maintain a twin pole structure. The property of  $f_0(600)$  and  $K_0^*(800)$  is also reinvestigated and previous results obtained in the single case is confirmed.

This paper is organized as follows: This section is the introduction, in section 2 we give a brief introduction to the perturbation calculation of  $\pi\pi \rightarrow K\bar{K}$ ,  $\pi\pi \rightarrow \pi\pi$ ,  $K\bar{K} \rightarrow K\bar{K}$ ,  $\pi\eta \rightarrow \pi\eta$ , and  $\pi\eta \rightarrow K\bar{K}$  scattering amplitudes as well as partial wave projection and Padé unitarization. In section 3 We fit the experimental phase shift and inelasticity to fix the LECs and extract pole positions. Section 4 devotes to the study of the property of poles by analyzing their  $N_c$  trajectories. We make physical discussion and conclusion in section 6, including a comparison between our results and previous results found in the literature.

## 2 Scattering amplitudes up to $\mathcal{O}(p^4)$ and partial wave projections

### 2.1 Effective Lagrangian

At lowest order, the chiral lagrangian at  $\mathcal{O}(p^2)$  is

$$\mathcal{L}_2 = \frac{f_0^2}{4} \langle \partial_\mu U^\dagger \partial^\mu U + \mathcal{M}(U + U^\dagger) \rangle, \quad (1)$$

where  $\langle \rangle$  stands for the trace of the  $3 \times 3$  matrices built from  $U(\Phi)$  and  $\mathcal{M}$ ,

$$U(\Phi) = \exp\left(\frac{i\sqrt{2}}{f_0}\Phi\right), \quad (2)$$

where  $\Phi$  is expressed in terms of the Goldstone boson fields as

$$\Phi(x) = \begin{pmatrix} \frac{1}{\sqrt{2}}\pi^0 + \frac{1}{\sqrt{6}}\eta & \pi^+ & K^+ \\ \pi^- & -\frac{1}{\sqrt{2}}\pi^0 + \frac{1}{\sqrt{6}}\eta & K^0 \\ K^- & \bar{K}^0 & -\frac{2}{\sqrt{6}}\eta \end{pmatrix}. \quad (3)$$

The mass matrix  $\mathcal{M}$  is given by

$$\mathcal{M} = \begin{pmatrix} \hat{m}_\pi^2 & 0 & 0 \\ 0 & \hat{m}_\pi^2 & 0 \\ 0 & 0 & 2\hat{m}_K^2 - \hat{m}_\pi^2 \end{pmatrix} \quad (4)$$

in the isospin limit, where  $\hat{m}$  means bare masses.

The chiral lagrangian of  $\mathcal{O}(p^4)$  can be written as, [3]

$$\begin{aligned} \mathcal{L}_4 = & L_1 \langle \partial_\mu U^\dagger \partial^\mu U \rangle^2 + L_2 \langle \partial_\mu U^\dagger \partial_\nu U \rangle \langle \partial^\mu U^\dagger \partial^\nu U \rangle + \\ & L_3 \langle \partial_\mu U^\dagger \partial^\mu U \partial_\nu U^\dagger \partial^\nu U \rangle + L_4 \langle \partial_\mu U^\dagger \partial^\mu U \rangle \langle U^\dagger \mathcal{M} + \mathcal{M}^\dagger U \rangle + \\ & L_5 \langle \partial_\mu U^\dagger \partial^\mu U (U^\dagger \mathcal{M} + \mathcal{M}^\dagger U) \rangle + L_6 \langle U^\dagger \mathcal{M} + \mathcal{M}^\dagger U \rangle^2 + \\ & L_7 \langle U^\dagger \mathcal{M} - \mathcal{M}^\dagger U \rangle^2 + L_8 \langle \mathcal{M}^\dagger U \mathcal{M}^\dagger U + U^\dagger \mathcal{M} U^\dagger \mathcal{M} \rangle. \end{aligned} \quad (5)$$

### 2.2 Amplitudes

At  $\mathcal{O}(p^4)$  one has to calculate the diagrams shown in Fig. 1.  $T_4^T$  represents contributions coming from the  $\mathcal{L}_2$  ChPT lagrangian with six fields and a tadpole.  $T_4^U$  represents the loops constructed from  $\mathcal{L}_2$  vertices with four fields. These loops include contributions from s, t and u channels.  $T_4^P$  amounts for the  $\mathcal{O}(p^4)$  polynomial contribution coming from  $\mathcal{L}_4$  lagrangian. In addition, one needs to take into account renormalization of masses, decay constants and wave functions. The relations between  $m_P$  ( $P = \pi, K, \eta$ ) and  $\hat{m}$ , and the ones between  $f_P$  and  $f_0$  can be obtained from [3]. The scattering amplitudes have been given in [21], all of which are expressed in terms of  $f_\pi$ . As an exercise, we have recalculated all the 1-loop amplitudes  $\pi\pi \rightarrow \pi\pi$ ,  $\pi\pi \rightarrow \bar{K}K$ ,  $\bar{K}K \rightarrow \bar{K}K$ ,  $K\pi \rightarrow K\eta$  and  $\pi\eta \rightarrow \bar{K}K$  and confirm previous results found in the literature.

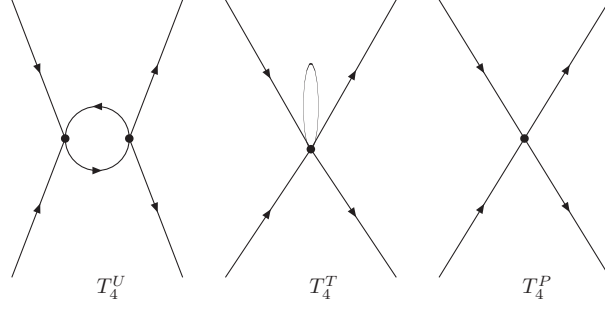


Figure 1: Feynman diagrams of  $\mathcal{O}(p^4)$

### 2.3 Partial wave expansion

The iso-spin decomposed amplitudes for  $\pi\pi \rightarrow \pi\pi$  scattering are

$$\begin{aligned} T^{I=0} &= T(\pi^0\pi^0 \rightarrow \pi^0\pi^0) + 2T(\pi^+\pi^- \rightarrow \pi^0\pi^0) , \\ T^{I=1} &= 2T(\pi^+\pi^- \rightarrow \pi^+\pi^-) - T(\pi^+\pi^- \rightarrow \pi^0\pi^0) - T(\pi^0\pi^0 \rightarrow \pi^0\pi^0) , \\ T^{I=2} &= T(\pi^0\pi^0 \rightarrow \pi^0\pi^0) - T(\pi^+\pi^- \rightarrow \pi^0\pi^0) ; \end{aligned} \quad (6)$$

for  $\pi\pi \rightarrow KK$  are

$$\begin{aligned} T^{I=0}(s, t, u) &= \sqrt{6}T(\pi^0\pi^0 \rightarrow K^+K^-) , \\ T^{I=1}(s, t, u) &= 2[T(\pi^+\pi^- \rightarrow K^+K^-) - T(\pi^0\pi^0 \rightarrow K^+K^-)] ; \end{aligned} \quad (7)$$

for  $KK \rightarrow KK$  scattering are

$$\begin{aligned} T^{I=0}(s, t, u) &= T(K^+K^- \rightarrow K^+K^-) + T(K^+K^- \rightarrow K^0\bar{K}^0) , \\ T^{I=1}(s, t, u) &= T(K^+K^- \rightarrow K^+K^-) - T(K^+K^- \rightarrow K^0\bar{K}^0) ; \end{aligned} \quad (8)$$

for  $\pi\eta \rightarrow \pi\eta$  scattering are

$$T^{I=1}(s, t, u) = T(\pi^0\eta \rightarrow \pi^0\eta) ; \quad (9)$$

and for  $\pi\eta \rightarrow KK$  scattering are

$$T_{12}^{I=1}(s, t, u) = -\sqrt{2}T(\pi^0\eta \rightarrow K^+K^-) . \quad (10)$$

The projection in definite angular momentum  $J$  is given by

$$T^{(I,J)} = \frac{1}{32N\pi} \int_{-1}^1 d(\cos\theta) T^I(s, t) P_J(\cos\theta) , \quad (11)$$

where  $N=2$  for elastic  $\pi\pi$  and  $\eta\eta$  scatterings, and  $N=1$  for other states. As an exercise we have re-calculated all of the above amplitudes and confirm the previous results found in the literature.

## 2.4 Padé approximation

In two-channel case, the unitarity condition reads,

$$\begin{aligned}\text{Im}T_{11} &= T_{11}\rho_1 T_{11}^* \theta(s - 4m_\pi^2) + T_{12}\rho_2 T_{21}^* \theta(s - 4m_K^2) , \\ \text{Im}T_{12} &= T_{11}\rho_1 T_{12}^* \theta(s - 4m_\pi^2) + T_{12}\rho_2 T_{22}^* \theta(s - 4m_K^2) , \\ \text{Im}T_{22} &= T_{21}\rho_1 T_{12}^* \theta(s - 4m_\pi^2) + T_{22}\rho_2 T_{22}^* \theta(s - 4m_K^2) ,\end{aligned}\quad (12)$$

where the  $IJ$  superscripts have been suppressed for simplicity.  $\rho_i = 2q_i/\sqrt{s}$  is the phase space function, with  $q_i$  the center of mass momentum in the state  $i$ . Here, for  $I,J=0,0$  and  $1,1$  channel, the subscript 1 represents for  $\pi\pi$ , 2 for  $\bar{K}K$ . The third equation only holds true above  $4m_K^2 - 4m_\pi^2$  along the real axis rather than above  $4m_\pi^2$  [22]. The  $[1,1]$  matrix Padé approximant reads,

$$T = T^{(2)} \cdot [T^{(2)} - T^{(4)}]^{-1} \cdot T^{(2)} . \quad (13)$$

However, it will cause the difficulty that the left hand cut  $(-\infty, 4m_K^2 - 4m_\pi^2]$  will appear not only in  $T_{22}$ , but also in the other two amplitudes as well. This difficulty also happens in couple channel K-Matrix parametrization [23]. Hence, Eq. (12) is satisfied exactly only above  $\bar{K}K$  threshold, although the deviation from unitarity may be numerically small in some cases [24].

Partial wave  $S$  matrix elements are given by

$$\begin{aligned}S_{11} &= 1 + 2i\rho_1(s)T_{11}(s) , \\ S_{12} &= 2i\sqrt{\rho_1(s)\rho_2(s)}T_{12}(s) \\ S_{22} &= 1 + 2i\rho_2(s)T_{22}(s) .\end{aligned}\quad (14)$$

In the physical region above the second threshold, the phase shifts and inelasticity can be related to T-matrix through the well-known parametrization,

$$S = \begin{pmatrix} \eta e^{2i\delta_1} & i\sqrt{1-\eta^2}e^{i(\delta_1+\delta_2)} \\ i\sqrt{1-\eta^2}e^{i(\delta_1+\delta_2)} & \eta e^{2i\delta_2} \end{pmatrix} . \quad (15)$$

When discussing  $\pi\pi$  scatterings, there have been many discussions in the literature on Padé approximation and its variations. This method is remarkable and is very helpful in some aspects, e.g., it builds a unitary scattering amplitude naturally from a perturbative one, it correctly predicts the existence of  $\sigma$ ,  $\kappa$  resonances at qualitative level, etc.. Nevertheless the unitarization method also maintains severe deficiencies, e.g., it violates crossing symmetry and introduces spurious poles on the complex  $s$ -plane and hence violates analyticity. Therefore we try to be careful when making conclusions on outputs from a Padé amplitudes.

## 3 Fit results and $N_c$ trajectories

In this part we will present two types of fits. In Fit I we fit in  $I,J=0,0$  and  $I,J=1,1$   $\pi\pi$ ,  $\bar{K}K$  couple channel data. This enables us to focus on physics of

$f_0(600)$  and  $f_0(980)$ . In Fit II we extend the above fit by including I,J=2,0 channel  $\pi\pi$  elastic scattering data and I,J=1,0  $\pi\eta \rightarrow \bar{K}K$  data. The latter is very important when exploring physics of  $a_0(980)$ .

### 3.1 Fit 1

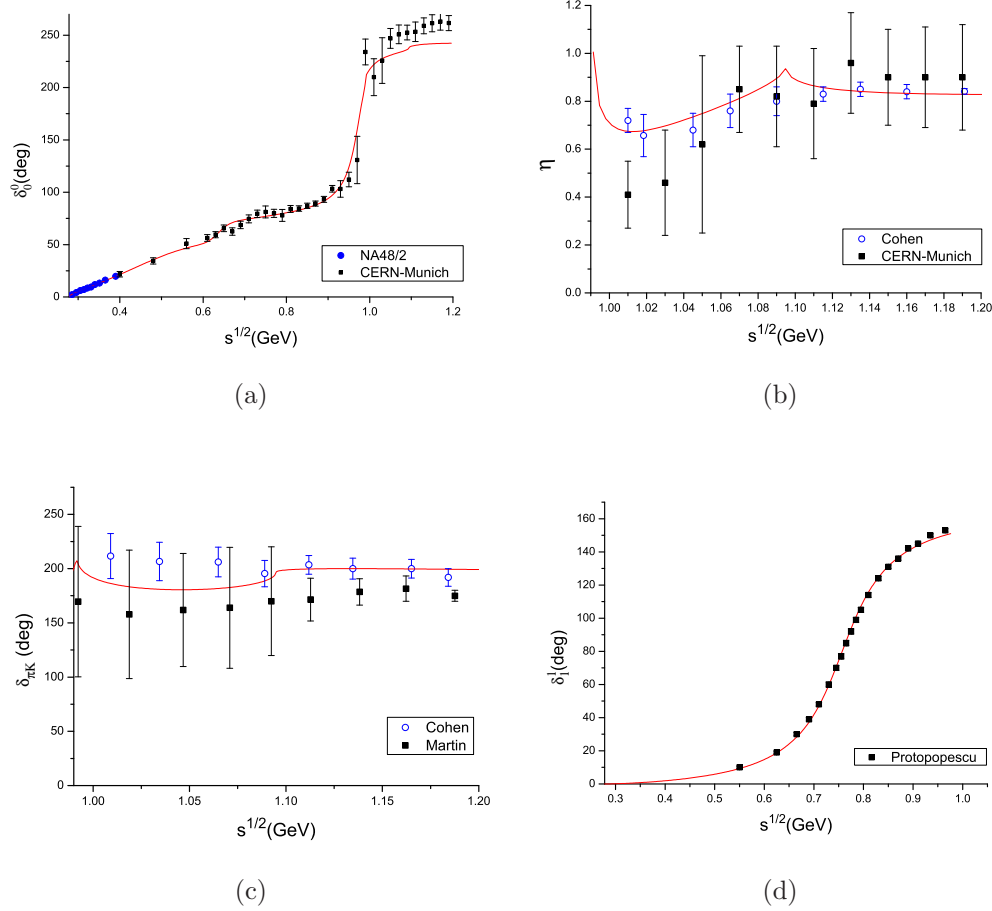


Figure 2: From Fit I: a)  $I = 0$  S wave  $\pi\pi$  phase shift; b) inelasticity; c)  $\delta_{\pi K}$ ; d) I,J=1,1 channel  $\pi\pi$  phase shift.

We first concentrate on  $\pi\pi, \bar{K}K$  couple channel system and the properties of  $\sigma$  and  $f_0(980)$ . The data sets are taken from [25]-[28] for I,J=0,0 channel (fit range from threshold to 1.2GeV) and [29] for I,J=1,1 channel (fit range from threshold to 1.0GeV). The fit results are shown in Fig. 2 with  $\chi^2_{d.o.f} = 186.3/95 = 1.96$ , and the LECs are given by Tab. 1. The  $\pi\pi$  scattering length of I,J=0,0 channel is

$$a_0^0 = 0.213m_\pi^{-1}. \quad (16)$$

	Fit I	Fit II	CHPT	Nc order
$L_1$	$0.98 \pm 0.06$	$1.25 \pm 0.02$	$0.40 \pm 0.3$	$\mathcal{O}(N_c)$
$L_2$	$1.39 \pm 0.06$	$1.63 \pm 0.03$	$1.35 \pm 0.3$	$\mathcal{O}(N_c)$
$L_3$	$-3.65 \pm 0.11$	$-4.07 \pm 0.02$	$-3.5 \pm 1.1$	$\mathcal{O}(N_c)$
$L_4$	$0.40 \pm 0.03$	$0.30 \pm 0.02$	$-0.30 \pm 0.5$	$\mathcal{O}(1)$
$L_5$	$0.21 \pm 0.73$	$-1.44 \pm 0.42$	$1.40 \pm 0.5$	$\mathcal{O}(N_c)$
$L_6$			$-0.2 \pm 0.3$	$\mathcal{O}(1)$
$L_7$			$-0.40 \pm 0.20$	$\mathcal{O}(1)$
$L_8$			$0.90 \pm 0.30$	$\mathcal{O}(N_c)$
$2L_6 + L_8$	$1.42 \pm 0.41$	$0.32 \pm 0.13$		
$2L_7 + L_8$		$1.38 \pm 0.38$		

Table 1: Low energy constants( $\times 10^{-3}$ ) and  $N_c$  dependence.

Pole positions of  $\sigma(600)$  and  $f_0(980)$  on the second sheet of  $\sqrt{s}$  plane are

$$\sqrt{s_\sigma} = (0.444 - 0.245i)\text{GeV}, \quad \sqrt{s_{f_0}} = (0.974 - 0.026i)\text{GeV}, \quad (17)$$

which are in agreement with recent determinations [7]-[9].

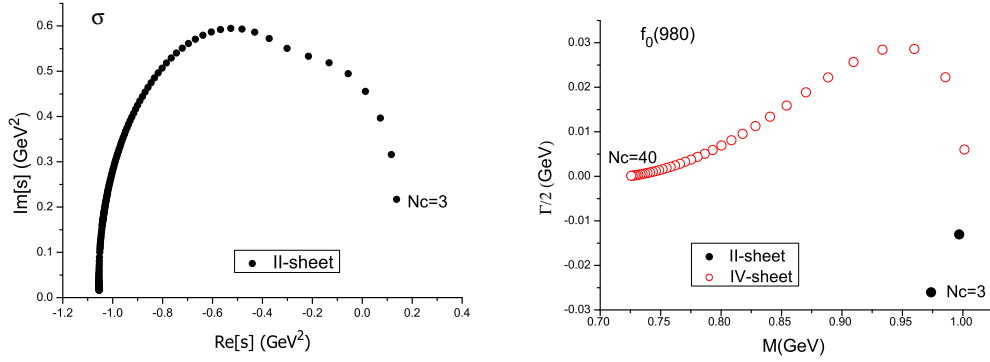


Figure 3:  $N_c$  trajectories of  $\sigma$ (left) and  $f_0(980)$ (right). Full circle: on sheet II; open circle: on sheet IV

We numerically trace the resonance pole positions when  $N_c$  varies. The  $N_c$  trajectories of  $\sigma$  and  $f_0(980)$  are shown in Fig. 3. We find that the  $\sigma$  pole will move towards negative real axis on the complex  $s$  plane when  $N_c$  is large enough. This result is previously observed using single channel [1,1] Padé amplitude [18].<sup>4</sup> This odd trajectory of  $f_0(600)$  makes the topic very puzzling and interesting, which certainly deserves further investigations. Actually the

<sup>4</sup>This phenomenon is also found in [20].

pole's destination in large  $N_c$  and chiral limit can be determined in the single channel approximation [18]:

$$s_\sigma = \frac{3f_\pi^2}{(44L_1 + 28L_2 + 22L_3)} . \quad (18)$$

In theory, this analytic solution also gives other two possibilities: fall down to the positive real axis, or move to infinity, by slightly tuning parameters. In the more complicated couple channel case, analytic solution of  $\sigma$  pole position is not available. However we have performed a limited numerical tests by varying LECs and did not find other possibilities except falling down to negative real axis. Nevertheless, in [1,2] Padé approximant it is found that the  $\sigma$  pole trajectory fall down on the positive real axis at roughly  $s_\sigma \sim 1\text{GeV}$  [18]. So the only robust conclusion one can make on the trajectory is that, unlike the  $\rho$  trajectory, the scalar one does not like to fall down to its fateful destination – the real axis.

It is more important to stress that, it is actually understood well what is the condition in obtaining Eq. (18), which reveals partly the secret hidden in Padé approximation. Using the PKU dispersive representation one obtains the same result as Eq. (18) under two additional assumptions: 1) neglect all crossed channel resonance exchanges (which contribute at leading order in  $1/N_c$  expansion); 2) assume in  $s$  channel there is only one pole involves [30].

The trajectory of  $f_0(980)$  is quite different. The  $f_0(980)$  pole moves into upper half plane of sheet IV from the lower half of sheet II in the  $\sqrt{s}$ -plane, winding around the branch point at the  $K\bar{K}$  threshold. But, it will fall on the positive real axis, above  $\pi\pi$  threshold but below  $\bar{K}K$  threshold on sheet IV eventually. This observation is not found in previous literature. In Ref. [19], it is also noticed that  $f_0(980)$  pole moves from sheet II to sheet IV, but jump to a quick conclusion that the pole moves to infinity without tracing the trajectory for larger value of  $N_c$ . If our result is correct then it predicts the following picture: when  $N_c = 3$  since  $f_0(980)$  lies on sheet II, it is a  $\bar{K}K$  bound state if  $\pi\pi$  channel is switched off, the destination of  $f_0(980)$  indicates that it be a virtual bound state of  $\bar{K}K$  when  $N_c$  becomes large. The conclusion is based on Morgan's pole counting mechanism [31], since no other poles near the  $\bar{K}K$  threshold are found.<sup>5</sup>

## 3.2 Fit 2

In Fit II we further include I,J=2,0 channel of  $\pi\pi \rightarrow \pi\pi$  [25] and I,J=1,0 channel of  $\pi\eta \rightarrow K\bar{K}$  [33]. For the latter, we use the  $\pi\eta$  effective mass distribution data from the  $pp \rightarrow p(\eta\pi^+\pi^-)p$  reaction studied by WA76 Collaboration [33], and the same formula as [21],

$$\frac{d\sigma}{dE_{cm}} = cp_{\pi\eta}|T_{\pi\eta \rightarrow K\bar{K}}^{I,J=1,0}|^2 + \text{background} , \quad (19)$$

---

<sup>5</sup>This technique is also used to support that the X(3872) be mainly a  $\bar{q}q$  state [32].



Channel (I,J)	Our results	ChPT $\mathcal{O}(p^4)$ [35]	ChPT $\mathcal{O}(p^6)$ [36]	Experiment [37]
(0,0)	0.208	0.20	$0.220 \pm 0.005$	$0.26 \pm 0.05$
(1,1)	0.036	0.037	$0.038 \pm 0.002$	$0.038 \pm 0.002$
(2,0)	-0.039	-0.042	$-0.042 \pm 0.010$	$-0.028 \pm 0.012$
(1,0)	0.004	0.007		
$(\frac{1}{2}, 0)$	0.169	0.17		0.13 to 0.24
$(\frac{1}{2}, 1)$	0.039	0.014		0.017 to 0.018
$(\frac{3}{2}, 0)$	-0.058	-0.05		-0.13 to -0.05

Table 2: From Fit II: scattering lengths, in unit of  $m_\pi^{-1}$  for S-wave and  $m_\pi^{-3}$  for P-wave.

Resonance	II	III	IV
$\sigma$	$0.457 - i0.242$		
$f_0(980)$	$0.974 - i0.025$		
$a_0(980)$		$0.640 - i0.002$	$1.131 - i0.079$
$\rho(770)$	$0.740 - i0.069$	$0.782 - i0.056$	
$(I, J) = (2, 0)$	$0.045m_\pi^2$		
$\kappa(800)$	$0.673 - i0.254$		
$K^*(892)$	$0.895 - i0.026$	$0.921 - i0.021$	

Table 3: Resonance pole positions on  $\sqrt{s}$  plane in unit of GeV, and virtual pole position on s plane.

where  $c$  is a normalization factor. The fit results are shown in Fig. 4 and Tab. 1, with  $\chi^2_{d.o.f} = 482/133 = 3.6$ . The background is subtracted in Fig. 4 (f) [21, 34]. The LECs and scattering lengths for different channels are given by Tab. 2, which are in agreement with  $\chi$ Pt [35, 36] and experimental results [37]. Notice that by fitting meson-meson scattering data, we can not determine  $L_6^r$ ,  $L_7^r$  and  $L_8^r$  individually, since these three parameters enter into the scattering amplitudes as the combination  $2L_6^r + L_8^r$  and  $2L_7^r + L_8^r$ . In the I,J=2,0 channel there is a virtual state. The pole position is at  $s_v = 0.045m_\pi^2$  on the II-sheet. A quite similar result has been given in [6].

In this paper we do not fit the data in I,J= $\frac{1}{2}, 0$ ;  $\frac{1}{2}, 1$  and I,J= $\frac{3}{2}, 0$   $K\pi \rightarrow K\pi$  channels. Rather, we give predictions on the phase shifts, scattering lengths in Fig. 5 and Tab. 2 respectively, which are in fairly good agreement with the experimental results. We also give predictions on pole positions of  $K_0^*(800)$  and  $K^*(892)$  when  $N_c = 3$ , as well as the trajectories when  $N_c$  varies, as shown in Fig. 6(b and f). In the following we briefly summarize the major physical results.

Firstly, the results unambiguously indicate that  $K^*(892)$  and  $\rho(770)$  are

Breit-Wigner particles as they move to the real axis of the complex  $\sqrt{s}$ -plane, on sheet II, where they meet their shadow partners on sheet III. Their masses and widths behave as  $\mathcal{O}(1)$  and  $\mathcal{O}(1/N_c)$  respectively in large  $N_c$  limit, as expected for normal  $q\bar{q}$  states. It is firstly observed in [15] that  $\rho$  and  $K^*$  behave as conventional  $\bar{q}q$  states in the unitarized amplitude since they fall down to the real axis straightforwardly. But the twin pole structure of these two particles was not discussed before. Hence the finding made in the present paper certainly put the previous observation on a more solid ground. This progress is important in the sense that it demonstrates that Padé approximants do faithfully reproduce the correct analytical structure of a Breit–Wigner resonance.

The  $N_c$  trajectory of  $\sigma(600)$  is quite similar to what we find in Fit 1, and  $K_0^*(800)$  has very similar trajectory comparing with that of  $f_0(600)$ , not to mention that they both have low masses and broad widths. We have made careful numerical tests and did not find shadow poles related to these two poles. This means that  $\sigma$  and  $\kappa$  basically only involve in single channel scattering.

The  $N_c$  trajectory of  $f_0(980)$  is also very similar to that in Fit I. Again, careful numerical analysis is made and we find no shadow pole associated with it.

For  $a_0(980)$ , see table 3, we find a sheet IV pole which is not too far away from  $K\bar{K}$  threshold. located at  $\sqrt{s} = 1.131 - i0.079\text{MeV}$ , Its location is not quite the same as the experimentally observed  $a_0(980)$ , but we do not take this discrepancy seriously since it may well be ascribed to the lack of enough good data in this channel. What is truly surprising is that, drastically different from  $f_0(980)$ , we find a companion shadow pole for  $a_0(980)$  on sheet III. Although far away from the physical region when  $N_c = 3$ , as shown in Fig. 6(d), both of them will move to negative real axis, on sheet IV (or sheet III). Large  $N_c$  techniques shows its powerfulness here as it can pinpoint the same origin of two totally different looking poles.<sup>6</sup> The twin pole structure uncovers the nature of  $a_0(980)$  as a Breit–Wigner resonance.<sup>7</sup>

## 4 Discussions and Conclusions

In this paper we have made efforts in exploring physics beyond the the validity domain of  $\chi\text{PT}$ , by studying  $[1,1]$  matrix Padé amplitudes. Masses and widths of resonances in all channels except  $a_0(980)$  are very well reproduced. We propose to study the shadow pole structure of a resonance, which is not emphasized in previous literature. We believe that this method enables us to avoid as much as possible model dependence. It is very encouraging to see,

---

<sup>6</sup>The pole counting mechanism no longer works well for the present situation since we encounter a strongly coupled system while the original pole counting argument requires a weakly coupled CDD pole [31].

<sup>7</sup>Nevertheless falling down to the negative real axis on sheet IV makes it difficult to be recognized. Here we remind again that the situation may be like the  $\sigma$  pole, i.e., its pole destination may be parameter dependent.

for the first time in the literature, that Padé approximants do faithfully exhibit the twin pole structure of  $\rho(770)$  and  $K^*(892)$  – particles widely accepted as standard Breit–Wigner resonances, or  $\bar{q}q$  states. This, in our point view, also shed lights and strengthen the level of confidence on the study of scalar resonances within Padé unitarization approach.

We trace numerically all poles’ trajectories when  $N_c$  varies. We find that  $\sigma$  and  $\kappa$  have quite similar  $N_c$  trajectories. They will move far away from the real axis on complex s-plan at first, but eventually fall down to real axis when  $N_c$  is large enough. This confirms the previous results on  $\sigma$  [18] and for  $\kappa$  the present result is quite new. The present result on  $\sigma$  also agrees with that of [20], but for  $\kappa$  pole the result is quite different. The absence of shadow pole suggests that the  $\sigma$  resonance is a pure  $SU(2)$  particle, i.e., does not contain  $\bar{s}s$  component.

The result of  $f_0(980)$  is also interesting. The sheet II pole will move to the real axis of IV-sheet above  $\pi\pi$  threshold, winding around the branching point of  $K\bar{K}$  threshold. This suggests that  $f_0(980)$  may be regarded as a molecular state in reality and gradually becomes a virtual bound state when  $N_c$  becomes large.

It is awesome to see that a twin pole structure of  $a_0(980)$  is also found even though it behaves quite oddly when  $N_c$  becomes large. If the picture shown in this paper is correct then the  $a_0(980)$  may be explained as a couple channel Breit–Wigner or  $\bar{q}q$  state. Notice that the conclusion reached in this paper is compatible with the picture drawn in Ref. [40] where it is found that  $a_0(980)$  is more ‘elementary’ than  $f_0(980)$ . Also the present result is compatible with the result of Ref. [41] where it is suggested that it is not possible to put  $f_0(980)$  into a  $\bar{q}q$  octet.

Predictions from Padé approximants may be model and parameter dependent. Its pole structure, on the contrary, is expected to be immune from these deficiencies. We hope that the exploration made in this this paper would stimulate more fruitful studies in future in exploring the properties of light scalars which is certainly interesting and challenging.

## 5 Acknowledgement

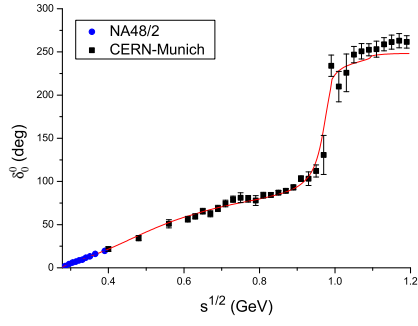
This work is supported in part by National Nature Science Foundations of China under contract number 10925522, 10875001 and 11021092.

## References

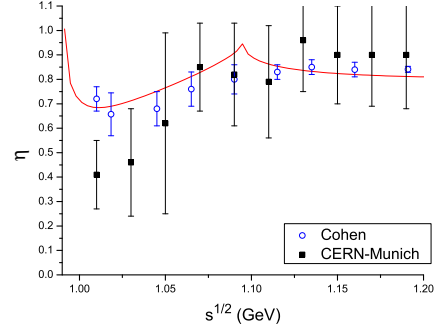
- [1] S. Weinberg, *Physica* **A96** (1979) 327.
- [2] J. Gasser, H. Leutwyler, *Ann. Phys. (NY)* **158** (1984) 142.
- [3] J. Gasser, H. Leutwyler, *Nucl. Phys.* **B250** (1985) 465.

- [4] Z. G. Xiao, H. Q. Zheng, Nucl. Phys. **A695** (2001) 273.
- [5] Z. Y. Zhou, H. Q. Zheng, Nucl. Phys. **A775** (2006) 212; H. Q. Zheng, *et al.*, Nucl. Phys. **A733** (2004) 235.
- [6] Z. Y. Zhou *et al.*, J. High Energy Phys. 02 (2005) 043.
- [7] I. Caprini, G. Colangelo, H. Leutwyler, Phys. Rev. Lett. **96** (2006) 132001.
- [8] S. Descotes-Genon, B. Moussallam, Eur. Phys. J. **C48** (2006) 553.
- [9] R. Kaminski, J. R. Pelaez, F. J. Yndurain, Phys. Rev. **D77** (2008) 054015.
- [10] M. R. Pennington, Invited talk at YKIS Seminar on New Frontiers in QCD: Exotic Hadrons and Hadronic Matter, Kyoto, Japan, 20 Nov-8 Dec 2006. Prog. Theor. Phys. Suppl. 168 (2007) 143.
- [11] N. N. Achasov, G. N. Shestakov, Phys. Rev. **D77** (2008) 074020.
- [12] G. Mennessier, S. Narison, W. Ochs, Phys. Lett. **B665** (2008) 205.
- [13] Yu. Mao, *et al.*, Phys. Rev. **D79** (2009) 116008.
- [14] G. Mennessier, S. Narison, X. G. Wang, Phys. Lett. **B688** (2010) 59; G. Mennessier, S. Narison, X. G. Wang, Phys. Lett. **B696** (2011) 40.
- [15] J. R. Pelaez, arXiv:0306063[hep-ph]; AIP Conf. Proc. 687 (2003) 74.
- [16] J. R. Pelaez, Phys. Rev. Lett. 92 (2004) 102001.
- [17] J. R. Pelaez and G. Rios, Phys. Rev. Lett. 97 (2006) 242002.
- [18] Z. X. Sun *et al.*, Mod. Phys. Lett. **A22** (2007) 711.
- [19] M. Uehara, hep-ph/0404221.
- [20] Z. H. Guo, J. A. Oller, arXiv:1104.2849[hep-ph].
- [21] A. G. Nicola, J. R. Pelaez, Phys. Rev. **D65** (2002) 054009.
- [22] J. Kennedy, T. D. Spearman, Phys. Rev. **126** (1962) 1596.
- [23] M. Aguilar-Benitez *et al.*, Nucl. Phys. **B140** (1978) 73.
- [24] F. Guerrero, J. A. Oller, Nucl. Phys. **B537** (1999) 459.
- [25] W. Ochs, Ph.D. thesis, Munich Univ., 1974.
- [26] J. R. Batley *et al.*, Eur. Phys. J. **C52** (2007) 875.
- [27] D. Cohen *et al.*, Phys. Rev. **D22** (1980) 2595.
- [28] A. D. Martin and E. N. Ozmurtu, Nucl. Phys. **B158** (1979) 5201.

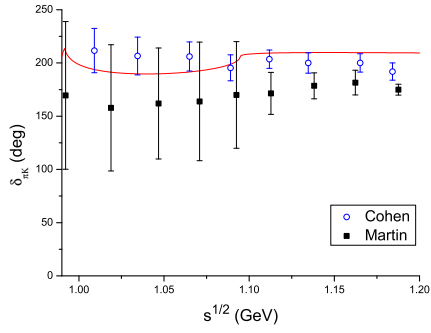
- [29] S. D. Protopopescu and M. Alson-Granjost, Phys. Rev. **D7** (1973) 1279.
- [30] Z. H. Guo, J. J. Sanz Cillero, H. Q. Zheng, JHEP **0706** (2007) 030.
- [31] D. Morgan, Nucl. Phys. **A543** (1992) 632.
- [32] Ou Zhang, C. Meng, H. Q. Zheng, Phys. Lett. **B680** (2009) 453.
- [33] T.A. Armstrong *et al.*, Z. Phys. **C52** (1991) 389.
- [34] S.M. Flatté, Phys. Lett. **B63** (1976) 224.
- [35] V. Bernard, N. Kaiser, U. G. Meissner, Nucl. Phys. **B357**(1991)129; Nucl. Phys. **B364** (1991) 283.
- [36] J. Bijnens, G. Colangelo and P. Talavera, J. High Energy Phys. **05** (1998) 014.
- [37] M.M. Nagels *et al.*, Nucl. Phys. **B147** (1979) 189.
- [38] P. Estabrooks *et al.*, Nucl. Phys. **B133** (1978) 490.
- [39] D. Linglin *et al.*, Nucl. Phys. **B57** (1973) 64.
- [40] V. Baru, J. Haidenbauer, C. Hanhart, Yu. Kalashnikova, A. Kudryavtsev, Phys. Lett. **B586** (2004) 53.
- [41] M. X. Su, L. Y. Xiao, H. Q. Zheng, Nucl. Phys. **A792** (2007) 288.



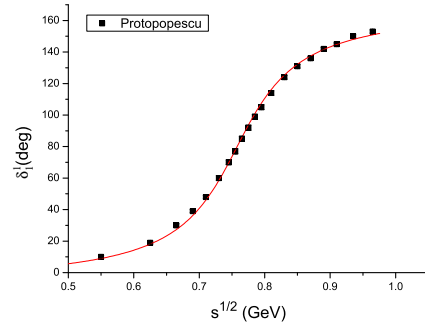
(a)



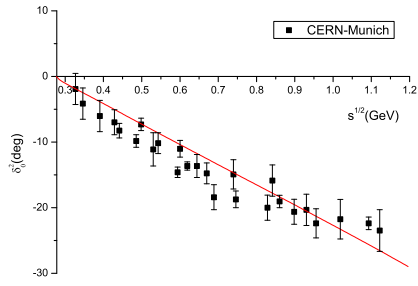
(b)



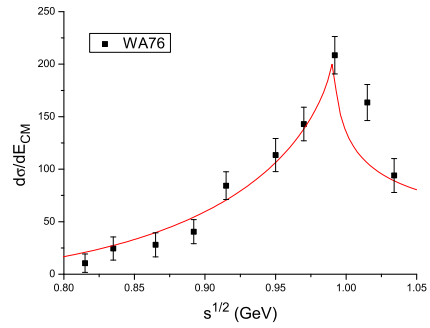
(c)



(d)



(e)



(f)

Figure 4: The results of Fit 2.

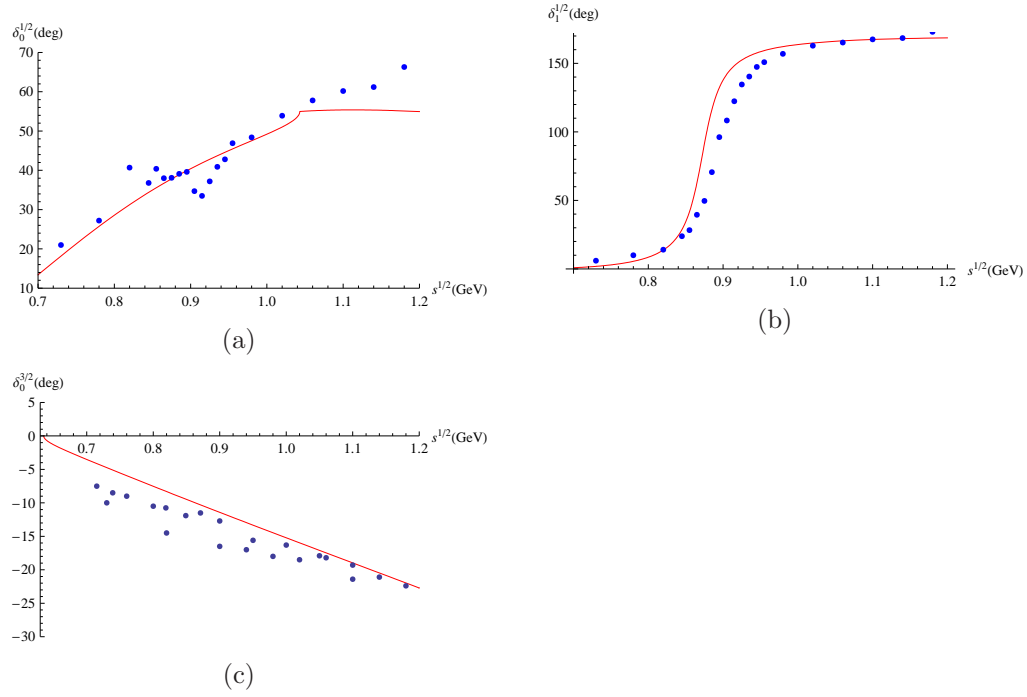
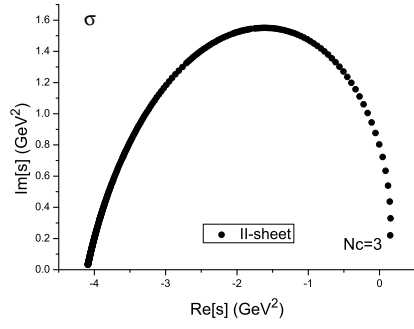
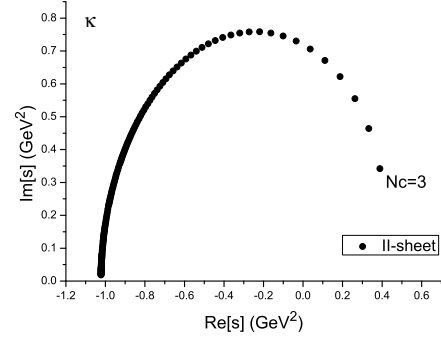


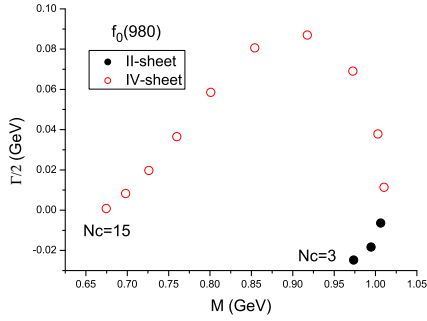
Figure 5: Predictions on phase shift from Fit 2. The data comes from [38, 39]



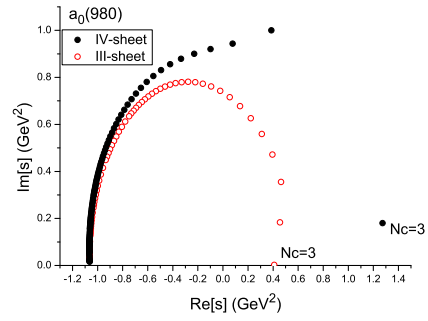
(a)



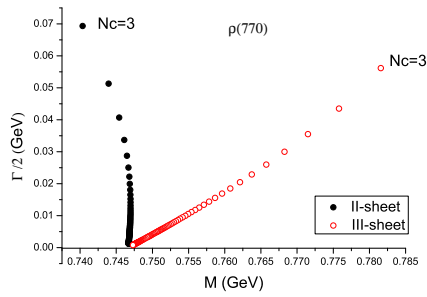
(b)



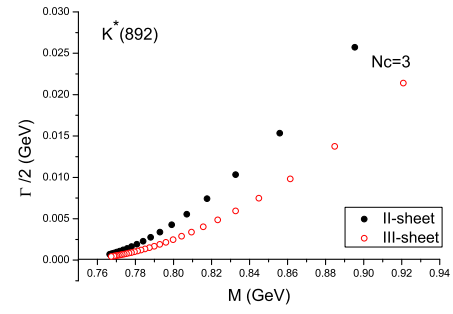
(c)



(d)



(e)



(f)

Figure 6:  $N_c$  trajectories of Fit 2.